MSWEP Retrospective

Version 2.1 documentation

Hylke Beck (hylkeb@princeton.edu)

Princeton University, Civil and Environmental Engineering, Princeton, NJ, United States

www.gloh2o.org

Contents

1 Introduction

This is the documentation for Multi-Source Weighted-Ensemble Precipitation (MSWEP) V2.1, a fully global precipitation (P) dataset (1979–2016) with a 3-hourly temporal and 0.1° spatial resolution. MSWEP takes advantage of the complementary strengths of gauge-, satellite-, and reanalysis-based data to provide reliable P estimates over the entire globe. MSWEP is available for download via `www.gloh2o.org`.

2 MSWEP V2.1 methodology

Figure 1 presents a flowchart outlining the main steps carried out to produce MSWEP V2.1. For each step, the reference to the subsection that provides detail is given between parentheses.

2a Gauge data quality control

Daily gauge observations were used to determine the merging weights and wet-day biases for the individual P datasets (Section 2d) and to improve the P estimates near gauge stations (Section 2i). Our initial database comprises 117 759 gauges worldwide compiled from the Global Historical Climatology Network-Daily (GHCN-D) database (Menne et al., 2012), the Global Summary of the Day (GSOD) database (`https://data.noaa.gov`), the Latin American Climate Assessment & Dataset (LACA&D) database (`http://lacad.ciifen-int.org`), the Chile Climate Data Library (`http://www.climatedatalibrary.cl`), and national databases for Mexico, Brazil, Peru, and Iran.

Gauge data can have considerable measurement errors and therefore quality control is important (Goodison et al., 1998, Viney and Bates, 2004, Sevruk et al., 2009, Schneider et al., 2014). For example, GSOD records frequently contain long series of erroneous zero rainfall. To identify and discard these periods, we developed an automated procedure entailing the following steps: (i) for each month, compute the fraction of days without P (fD); (ii) exclude months without any P ($fD = 1$), compute the distribution mean (μ) and standard deviation (σ); (iii) if the CDF of the normal distribution with μ and σ evaluated at $fD = 0.9$ exceeds 0.85, we consider the station to be sufficiently 'wet' for detecting the erroneous zeros and proceed to the next step; (iv) a year is marked as erroneous if the median of the 12 monthly fD values exceeds 0.9; and (v) the six months preceding and following each erroneous year are also marked as erroneous. Figure 2 illustrates the procedure for an arbitrarily selected GSOD station with the described issue.

In addition, we eliminated all days with $P > 2000$ mm, and discarded gauges with record length < 4 years during 1979–2016. From the remaining set of 68 707 gauges we also discarded those matching one or more of the following criteria (% of stations satisfying the criteria reported between parentheses): (i) 3-day Pearson correlation coefficient ($r_{3\,\mathrm{day}}$) computed between daily gauge and gridded data for both the ≤ 1999 and ≥ 2000 periods for all datasets < 0.4, and $r_{3\,\mathrm{day}}$ with the closest station < 0.4 (1.06 %); (ii) more than half of the 3-day intervals contain missing

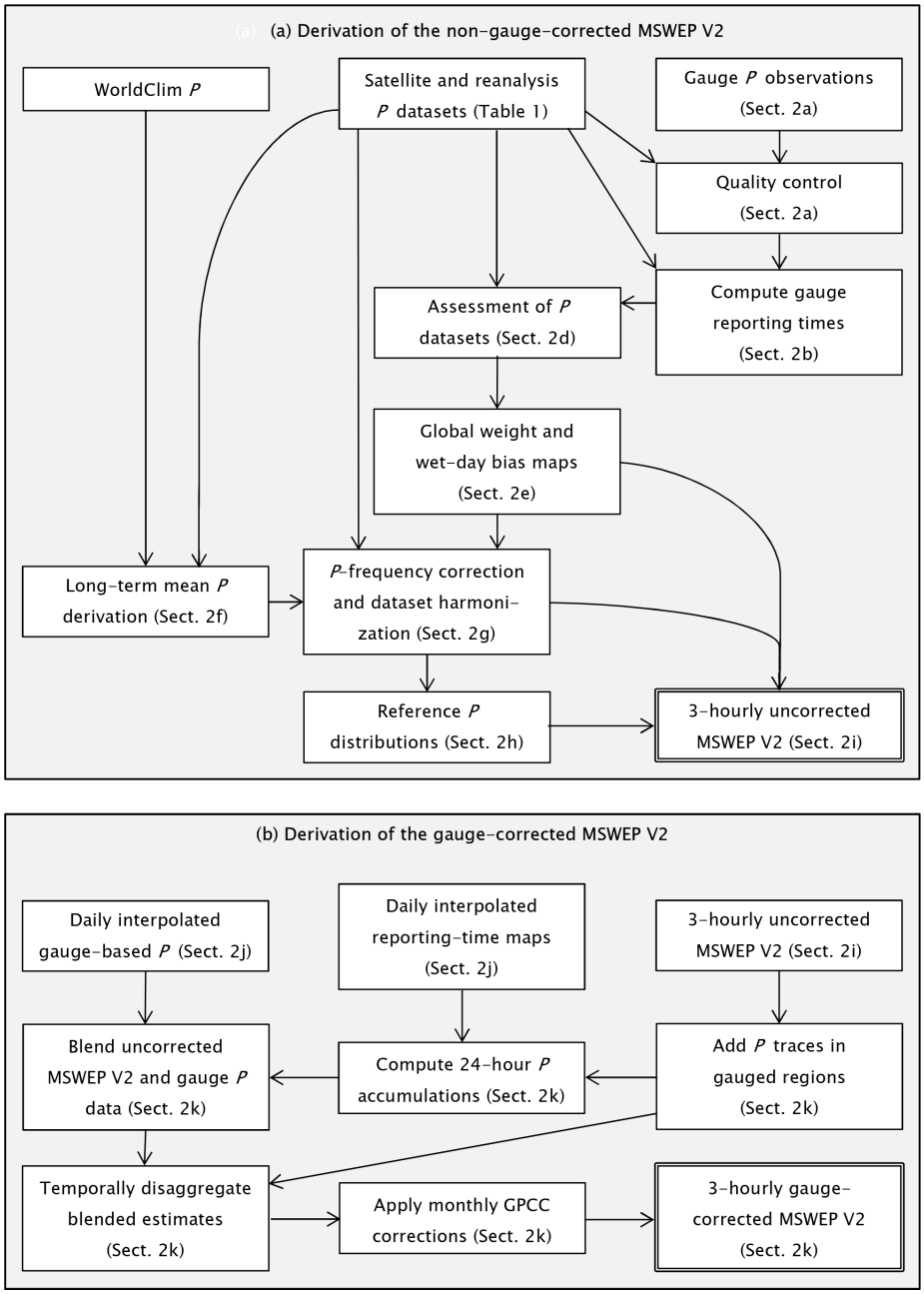

Figure 1: Flowchart outlining the main steps carried to produce the (a) uncorrected and (b) gauge-corrected MSWEP V2.1. For each step, the reference to the subsection that provides detail is given between parentheses.

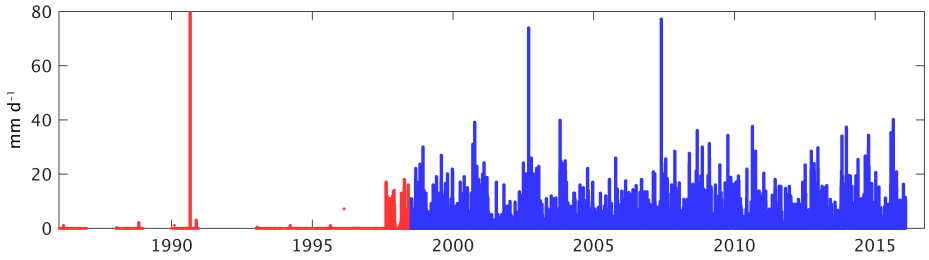

Figure 2: Daily P measured at GSOD station 038660 (50.58°N 1.30°W) with the automatically detected erroneous period indicated in red.

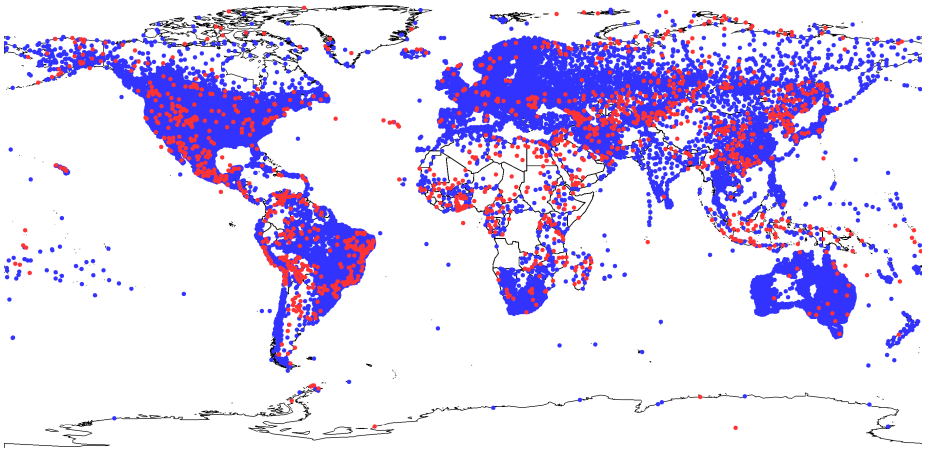

Figure 3: The gauges used to produce MSWEP in blue ($N = 66\,993$) and the discarded gauges in red ($N = 1714$).

values (1.04 %); (iii) less than 15 unique values in the entire record (0.19 %); and (iv) the highest and/or second highest values were present > 3 times in the record, indicative of truncated peaks (0.34 %). In total, 1714 (2.49 %) of the gauges fulfilled one or more of these criteria and hence were discarded, resulting in a final gauge dataset comprising 66 993 gauges (Figure 3).

2b Inferring gauge reporting times

Information about gauge reporting times is crucial to avoid timing mismatches when applying daily gauge corrections, but is generally not provided. We developed a procedure to infer gauge reporting times using 3-hourly satellite and reanalysis P datasets (CMORPH, ERA-Interim, GSMaP, and JRA-55; Table 1). Specifically, we calculated, for each gauge, Spearman rank correlation coefficients (ρ) between daily gauge- and dataset-based time series, with the dataset-based time series shifted by offsets of $-36, -33, -30, \ldots, +30, +33$, and $+36$ hours, resulting in $4 \times 25 = 100$ ρ

values for each gauge. The dataset and temporal-offset combination yielding the highest ρ value was subsequently taken to reflect the UTC boundary of the 24-hour accumulation period for the gauge under consideration. Note that this approach yields an estimate with, at best, a 3-hourly accuracy, and relies on the assumption of a temporally constant reporting time, which may not be true for every gauge.

2c Gauge-based assessment of satellite and reanalysis P datasets

MSWEP V2.1 incorporates six non-gauge-corrected gridded P datasets (Table 1). To assess the individual performance of these datasets, we calculated Pearson correlation coefficients between 3-day mean gauge- and dataset-based P time series ($r_{3\,\mathrm{day}}$) for the period 2000–2016. To minimize timing mismatches between the gauge- and dataset-based time series, prior to calculating the $r_{3\,\mathrm{day}}$ values, the records of gauges with reporting times $> +12$ hours UTC were shifted backward by -1 day, while the records of gauges with reporting times < -12 hours UTC were shifted forward by $+1$ day (Section 2b). The use of 3-day rather than daily averages has two benefits: first, it minimizes the impact of any remaining temporal mismatches in the 24-hour accumulation period between the datasets and the gauges; and second, it reduces the influence of days with potentially erroneous gauge measurements. The $r_{3\,\mathrm{day}}$ values were calculated for the full period of contemporaneous gauge- and dataset-based data, as well as for 'cold' and 'warm' conditions, distinguished using a daily mean air temperature (T_a) threshold of 5°C. MSWEP V1.1 employed a 1°C threshold, which we increased in V2.1 to further reduce the likelihood of incorporating potentially unreliable satellite data. For T_a, we used ERA-Interim (Dee et al., 2011) downscaled to 0.1° and offset to match the long-term mean of the high-resolution gauge-based WorldClim dataset (V2.0; Fick and Hijmans, 2017). We only calculated an $r_{3\,\mathrm{day}}$ value if > 1 year of simultaneous gauge and gridded 3-day means were available. The $r_{3\,\mathrm{day}}$ values range from -1 to 1, with higher values corresponding to better performance.

Reanalyses tend to overestimate P frequency and underestimate intensity due to deficiencies in the parameterization of the physical processes controlling P generation (Zolina et al., 2004, Sun et al., 2006, Lopez, 2007, Stephens et al., 2010, Skok et al., 2015, Herold et al., 2016). To quantify and correct for this, we calculated the bias in the number of wet days, using the gauge observations as reference, according to:

$$\beta_{\mathrm{WD}} = \frac{\mathrm{WD}_{\mathrm{dataset}}}{\mathrm{WD}_{\mathrm{gauge}}}, \tag{1}$$

where β_{WD} (unitless) is the bias in number of wet days, and $\mathrm{WD}_{\mathrm{dataset}}$ and $\mathrm{WD}_{\mathrm{gauge}}$ represent the number of wet days in the reanalysis and the gauge observations, respectively. β_{WD} values were calculated only if > 5 years of contemporaneous gauge- and reanalysis-based data were available. Wet days were identified using a 0.5 mm d^{-1} threshold, similar to several previous studies (e.g., Akinremi et al., 1999, Haylock et al., 2008, Driouech et al., 2009, Trenberth and Zhang, ress). $\mathrm{WD}_{\mathrm{dataset}}$ was computed from daily accumulations to be consistent with the gauge observations. β_{WD} values range from 0 to ∞, with values closer to unity corresponding to better performance.

Table 1: Overview of the (quasi-)global gridded *P* datasets used in this study. MSWEP V2.1 has been added for the sake of completeness. Datasets denoted by an asterisk in the first column were incorporated in MSWEP V2.1. Abbreviations: G=gauge; S=satellite; R=reanalysis; NRT=near real-time. In the spatial coverage column, "global" indicates fully global coverage including ocean areas, whereas "land" indicates that the coverage is restricted to the land surface.

Name	Details	Data source(s)	Spatial resolution	Spatial coverage	Temporal resolution	Temporal coverage	Reference(s)
CMORPH*	CPC MORPHing technique (CMORPH) V1.0 and V0.X RT	S	0.07°	60°N/S	30 minutes	1998–NRT[1]	Joyce et al. (2004)
ERA-Interim*	European Centre for Medium-range Weather Forecasts ReAnalysis Interim (ERA-Interim)	R	∼80 km	Global	3 hourly	1979–NRT[3]	Dee et al. (2011)
GPCC V7*	Global Precipitation Climatology Centre (GPCC) Full Data Reanalysis V7 extended using First Guess	G	0.5°/1°	Land	Monthly	1951–NRT[2]	Schneider et al. (2014, 2017)
GridSat*	Gridded Satellite (GridSat) B1 IR archive V02R01	S	0.1°	∼50°N/S	3 hourly	1983–2016	Knapp et al. (2011); this study (Appendix)
GSMaP*	Global Satellite Mapping of Precipitation (GSMaP) Moving Vector with Kalman (MVK) standard V5 and V6	S	0.1°	60°N/S	Hourly	2000–NRT[2]	Ushio et al. (2009)
JRA-55*	Japanese 55-year ReAnalysis (JRA-55)	R	∼60 km	Global	3 hourly	1959–NRT[2]	Kobayashi et al. (2015)
MSWEP V1.1	Multi-Source Weighted-Ensemble Precipitation (MSWEP) V1.1	G, S, R	0.25°	Land	3 hourly	1979–2015	Beck et al. (2017)
MSWEP V2.1	Multi-Source Weighted-Ensemble Precipitation (MSWEP) V2.1	G, S, R	0.1°	Global	3 hourly	1979–2016	This study
TMPA 3B42RT*	TRMM Multi-satellite Precipitation Analysis (TMPA) 3B42RT V7	S	0.25°	50°N/S	3 hourly	2000–NRT[1]	Huffman et al. (2007)

[1]Available until the present with a delay of several hours.
[2]Available until the present with a delay of several days.
[3]Available until the present with a delay of several months.

2d Global maps of weights and wet-day biases

Global weight maps were derived for the entire period and for warm and cold conditions for each of the non-gauge-based satellite and reanalysis P datasets (Table 1) from the gauge-based $r_{3\,\mathrm{day}}$ values (Section 2c). The $r_{3\,\mathrm{day}}$ values were truncated at zero, squared to yield the explained variance, and subsequently interpolated to yield gap-free global weight maps by calculating, for each 0.1° grid cell, the median of the 10 nearest gauges. The cold-condition weights were set to zero for the satellite datasets. Similarly, gap-free global maps of β_{WD} were produced for the reanalyses, to correct P frequency prior to the merging.

Due to a lack of gauges over ocean areas, the use of the 10 nearest gauges in the interpolation frequently resulted in strong discontinuities in the middle of oceans due to contrasting values on opposite sides of the oceans. To eliminate these discontinuities, we applied an exponential smoothing kernel with a bandwidth of 1000 km over the ocean areas of the interpolated weight and β_{WD} maps.

2e Determination of long-term mean P

The long-term mean P over the land surface was determined in V2.1 using the gauge-based WorldClim dataset (1-km resolution; V2.0; Fick and Hijmans, 2017) rather than the CHPclim dataset (0.05° resolution; Funk et al., 2015). We switched from CHPclim to WorldClim due to the better gauge coverage in South America, Scandinavia, India, Australia, and New Zealand. Similar to MSWEP V1.1, systematic P underestimation over land due to gauge under-catch and orographic effects was corrected by inferring catchment-average P using the Zhang et al. (2001) relationship in combination with river discharge (Q) observations and potential evaporation (E_{p}) estimates (Beck et al., 2017). However, for MSWEP V2.1, the correction factors inferred for Chilean and Iranian catchments were set to 1 prior to the interpolation, due to suspected issues with the observed Q data.

The long-term mean P over the oceans was estimated by weighting the long-term means of five satellite and reanalysis datasets (CMORPH, GSMaP, ERA-Interim, JRA-55, and TMPA 3B42RT; Table 1). The weights for the satellite datasets (w_{s}) were set to 1 for latitudes $< 20°$ and 0 for latitudes $> 40°$, decreasing linearly from 1 at 20° to 0 at 40°. The weights for the reanalyses (w_{r}) were set to $1 - w_{\mathrm{s}}$. Thus, w_{r} was set to 0 at latitudes $< 20°$, due to the tendency of reanalyses to overestimate tropical P amounts (Trenberth et al., 2011, Kang and Ahn, 2015).

2f P frequency correction and dataset harmonization

The following steps were carried out to reduce P frequency of the reanalyses and harmonize the datasets incorporated in MSWEP V2.1:

1. The datasets with spatial resolutions higher or lower than 0.1° (CMORPH, ERA-Interim, JRA-55, and TMPA 3B42RT) were resampled to 0.1° using nearest neighbor resampling, and 3-hourly means were calculated for the datasets with temporal resolutions < 3 hours (CMORPH and GSMaP).

2. The WATCH (Weedon et al., 2011) and WFDEI (Weedon et al., 2014) datasets (derived respectively from the ERA-40 and ERA-Interim reanalyses) were corrected for overestimations in P frequency by progressively removing the smallest events until the P frequency matched that of the gauge-based CRU dataset. However, this approach resulted in P distributions with a lack of light P events. We therefore employed an alternative approach to correct the P frequency of the reanalyses (ERA-Interim and JRA-55). First, for grid cells with interpolated β_{WD} values > 1, we calculated the 'correct' annual number of wet days ($\mathrm{WD}_{\mathrm{objective}}$) according to: $\mathrm{WD}_{\mathrm{objective}} = \mathrm{WD}_{\mathrm{dataset}}/\beta_{\mathrm{WD}}$, where $\mathrm{WD}_{\mathrm{dataset}}$ was calculated from daily accumulations and β_{WD} represents the interpolated value (Section 2d). Next, we iteratively carried out the following steps: (i) subtract d mm $3\mathrm{h}^{-1}$ from the original 3-hourly time series, starting with $d = 0.01$ mm $3\mathrm{h}^{-1}$; (ii) truncate the resulting values to zero and rescale them to restore the original long-term mean; (iii) calculate the annual number of wet days from daily accumulations ($\mathrm{WD}_{\mathrm{new}}$); (iv) return to step (i), increasing d in 0.01 mm $3\mathrm{h}^{-1}$ increments, until $\mathrm{WD}_{\mathrm{new}} \leq \mathrm{WD}_{\mathrm{objective}}$.

3. The reanalysis datasets, which are valid for the entire period, and the satellite datasets, which are only valid for warm conditions, were rescaled to minimize the presence of spurious temporal discontinuities after merging. For this purpose, we first rescaled the reanalyses to match the long-term P estimates derived in Section 2e. Next, means were calculated for the entire period and for warm and cold conditions based on the rescaled reanalyses, using the full-period weight maps derived in Section 2d. Finally, the satellite datasets were rescaled to match the rescaled warm-condition reanalysis mean.

2g Reference P distributions

In MSWEP V2.1, the 3-hourly merged satellite and reanalysis P estimates were CDF matched to reference P distributions (Figure 1), to correct the spurious drizzle and attenuated peaks evident in V1 (Nair and Indu, 2017, Zhang et al., 2017). Two separate 3-hourly reference distributions (0.1° resolution) were calculated, one representing warm conditions and one representing cold conditions (as before distinguished using a daily mean T_{a} threshold of 5°C). The reference distribution for warm conditions was calculated by weighted-median averaging of the distributions of five satellite and reanalysis P datasets (CMORPH, ERA-Interim, GSMaP, JRA-55, and TMPA 3B42RT; Table 1). The GridSat dataset was excluded because it does not represent an independent estimate, being derived using the reference distributions (Appendix). For cold conditions, the reference distribution was calculated by weighted-median averaging of only the two reanalysis P datasets (ERA-Interim and JRA-55). Prior to the averaging, the P frequency of the reanalyses was corrected and the datasets were homogenized as decribed in the previous section. We only used data more recent than 2000 to derive the reference distributions for two reasons: first, to avoid inconsistencies between the warm- and cold-condition reference distributions due to the much longer temporal coverage of the reanalyses; and second, because satellite data prior to the year 2000 tend have greater uncertainty (Xie et al., 2017).

2h Merging of satellite and reanalysis P datasets

Six gridded P datasets (CMORPH, ERA-Interim, GridSat, GSMaP, JRA-55, and TMPA 3B42RT; Table 1) were merged through the following steps:

1. For cold and warm conditions separately, and for every possible P dataset combination, the 3-hourly estimates were merged by weighted-mean averaging using the interpolated weight maps (Section 2d). The total number of combinations comprising two or more P datasets equals 57 for warm conditions, while just one combination (containing both reanalyses) is valid for cold conditions (the satellite data were discarded). Prior to the merging, the P frequency of the reanalyses was corrected and the datasets were harmonized (Section 2f). Satellite data were discarded prior to the year 2000 and for grid cells with daily mean $T_a \geq 5$°C less than 10 % of the time.

2. Averaging multiple data sources inevitably results in spurious drizzle and attenuated peaks, as was the case for MSWEP V1 (Nair and Indu, 2017, Zhang et al., 2017). To correct for this, we CDF matched the P estimates from 2000–2016 of each dataset combination, for cold and warm conditions separately, to the reference P distributions (which represent the period 2000–2016; see Section 2g). To obtain consistent time series for the entire 1979–2016 period, we first calculated the change in the P estimates due to the CDF corrections for different P magnitudes, after which we applied the same magnitude-specific changes to the P estimates from the 1979–1999 period. Figure 4 illustrates the impact of the CDF corrections.

3. For cold and warm conditions separately, and for each possible dataset combination, we subsequently calculated the cumulative interpolated weight, which roughly reflects the total information content of the dataset combination in question. Next, we selected, for each 3-hourly time step and 0.1° grid cell, the merged and CDF-corrected P value from the dataset combination with the highest cumulative weight. The CDF corrections applied in the previous step ensure that temporal transitions from one dataset combination to another are largely unnoticeable.

2i Gauge data interpolation

MSWEP V1.1 incorporated daily gauge data from CPC Unified (0.5° resolution; Xie et al., 2007, Chen et al., 2008) and monthly gauge data from GPCC V7 (0.5° resolution; Schneider et al., 2014). However, CPC Unified incorporates fewer quality-controlled observations than we have in our collection; on January 11, 2004, for example, the difference was 23 334 versus 30 695 observations. We therefore produced our own daily high-resolution (0.1°) gauge-based dataset to replace CPC Unified for MSWEP V2.1. We used the inverse-distance weighting (IDW) interpolation technique (Shepard, 1968, Dirks et al., 1998) in combination with quality-controlled observations from 66 993 gauges across the globe (Section 2a). The IDW technique was chosen for

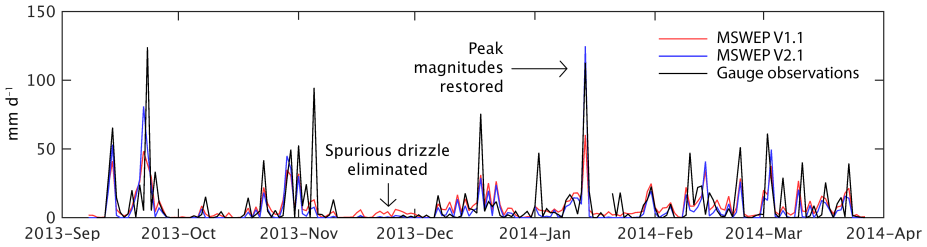

Figure 4: Daily P measured at GHCN-D station IOW00070701 (7.35°S 72.45°E), including time series from the non-gauge-corrected MSWEP V1.1 and V2.1, illustrating the effect of the frequency and CDF corrections introduced in V2.1.

its computational efficiency and superior performance in a comprehensive evaluation of six interpolation techniques in Brazil (Xavier et al., 2016).

For each day and each 0.1° grid cell, a P anomaly was calculated based on surrounding gauges according to:

$$X_{\text{int}\,j} = \frac{\sum_{i=1}^{n} X_{\text{obs}\,i}\; d_i^{-\lambda}}{\sum_{i=1}^{n} d_i^{-\lambda}}, \tag{2}$$

where $X_{\text{int}\,j}$ (unitless) is the interpolated P anomaly for grid cell j, $X_{\text{obs}\,i}$ (unitless) represents the gauge P anomaly (computated by dividing the original gauge estimates by their long-term mean), $i = 1, 2, \ldots, n$ denote the nearest gauges within a 1000-km radius (maximum ten), d_i (km) represents the distance between grid cell j and gauge i, and λ (unitless) is the distance-decay parameter. Gauges located $>$ 1000 km distance from the grid cell under consideration were assumed to have negligible influence and thus excluded. Although λ is known to vary depending on storm type and location, we used a fixed value of 3 following Garcia et al. (2008). Finally, the interpolated P anomalies were converted back to P depths by rescaling them to match the bias-corrected long-term mean P estimate derived previously (Section 2e).

In contrast to MSWEP V1.1, V2.1 accounts for regional differences in reporting times when applying the daily gauge corrections (Figure 1). For this purpose, we produced daily reporting-time maps based on the calculated reporting times (Section 2b). These maps were produced using Equation 2 with X redefined as the reporting time in UTC, at a coarser 1° resolution to reduce the computational time.

Daily weight maps (0.1° resolution) corresponding to the interpolated P data and monthly weight maps (0.5° resolution) corresponding to the GPCC data were estimated as a function of gauge density using the following expression:

$$W_l = 5\sqrt{\sum_{k=1}^{m} \exp\left(\frac{-D_k}{D_0}\right)\sqrt{s_k}}, \tag{3}$$

where W_l (unitless) represents the weight for grid cell l, $k = 1, 2, \ldots, m$ denote all the grid cells in a 1000-km radius of grid cell l (including grid cell l itself), D_k (km)

represents the distance between grid cells l and k, D_0 (km) represents the range of influence, and s_k (unitless) represents the number of stations in grid cell k. D_0 was set to 25 km using trial and error. The gauge weight equation is the same as in MSWEP V1.1 (Beck et al., 2017). The factor 5 is used here because the weight for the satellite- and reanalysis-based merged estimate was calculated in V2.1 by summing the weights of all datasets (Section 2h), while in V1.1 it was calculated by summing only the weights of the single satellite dataset that performed best and the single reanalysis dataset that performed best.

2j Gauge correction scheme

We first corrected the merged 3-hourly satellite- and reanalyis-based P estimates (referred to hereafter as p_{zero}; see Section 2h) using the daily 0.1° interpolated gauge data derived in the preceding section. We used a multiplicative rather than an additive gauge correction scheme (Vila et al., 2009), to preserve the sub-daily distribution of p_{zero}. However, very small P amounts were added to the p_{zero} estimates, to avoid a high gauge estimate from yielding a zero estimate after the correction when $p_{\text{zero}} = 0$, which occurs frequently in MSWEP V2.1 due to the P frequency and CDF corrections. Specifically, we added an almost negligable amount (0.1 %) of the non-CDF-matched (and thus drizzly) merged satellite- and reanalysis-based P data. The resulting estimate will be referred to hereafter as p_{nonzero}. Next, daily P accumulations of p_{nonzero} were calculated for the 24-hour period ending at the interpolated reporting time, after which a blended estimate was calculated by weighted-mean averaging of the daily p_{nonzero} accumulation and the daily interpolated gauge-based estimate (Section 2i). The blended estimate was subsequently temporally disaggregated using the 3-hourly p_{nonzero} data to yield $p_{\text{corr daily}}$, completing the daily gauge correction procedure. MSWEP is the only (quasi-)global P dataset besides GSMaP to apply daily gauge corrections.

The 3-hourly $p_{\text{corr daily}}$ data were corrected at the monthly time scale using the 0.5° GPCC V7 dataset (Schneider et al., 2014, 2017). For this purpose we first calculated monthly P accumulations of $p_{\text{corr daily}}$, after which we derived a monthly blended estimate using weighted-mean averaging. The weights associated with the monthly $p_{\text{corr daily}}$ accumulations were estimated by summing the p_{nonzero} weight (Section 2h) and the daily gauge weight (Section 2i). The 3-hourly $p_{\text{corr daily}}$ data were subsequently rescaled to match this blended estimate, completing the monthly gauge correction procedure and yielding the final gauge-corrected MSWEP V2.1. A flowchart illustrating the entire gauge correction procedure is shown in Figure 1.

3 Data format

MSWEP V2 is provided in the widely used netCDF-4 format at 3-hourly, daily, and monthly temporal resolution, and 0.1° and 0.5° spatial resolution. The 3-hourly and daily data are supplied as monthly files, while the monthly data are supplied as single files. The actual precipitation estimates are stored in the `precipitation` netCDF field (dimensions 1800 × 3600 for the 0.1° data and dimensions 360 × 720 for the

0.5° data) in mm/3-hour, mm/day, and mm/month units for the 3-hourly, daily, and monthly data, respectively.

4 Reading data

Precipitation data for a particular day (e.g., April 25, 2010) can be read using MATLAB as follows:

```
global_precip = ncread('201004.nc','precipitation',[1 1 25],[Inf Inf 1])';
```

The transposition accent is necessary because MATLAB incorrectly reorders the dimensions when opening netCDF files. The same data are read using Python as follows:

```
from netCDF4 import Dataset
dataset = Dataset('201004.nc', 'r')
global_precip = dataset.variables['precipitation'][24,:,:]
dataset.close()
```

Note that 24 instead of 25 is used for the slicing because Python starts indexing at zero.

5 Version history

Version 2.1 (November 20, 2017)

Two changes. Firstly, NCEP-CFSR precipitation data were removed due to the presence of spurious trends (NCEP-CFSR was added in version 2.0). Secondly, corrections using the monthly gauge-based GPCC precipitation dataset were reintroduced (these were removed in version 2.0).

Version 2.01 (October 8, 2017)

Fixed a mistake in the netCDF metadata. For all netCDF files, the units for the time variable were changed from "days since 1900-01-01 00:00:00" to "days since 1899-12-31 00:00:00". The actual time data have not been changed. In the case of the 3-hourly data, a (fictional) time value of, for example, 1.125 would indicate that the data represent the period 03:00Z to 05:59Z on January 1, 1900.

Version 2.0 (July 23, 2017)

Major upgrade containing numerous changes in the data sources as well as the merging algorithm, and as a result markedly different precipitation estimates, especially at the daily and 3-hourly time scales (notably less drizzle and higher peaks). The paper describing version 2 is currently in preparation. Both version 1 and 2 have been validated in Beck et al. (2017). The most important changes in version 2 include:

1. The correction of distributional precipitation biases to account for the spurious drizzle and attenuated peaks evident in previous versions of MSWEP.

2. Increasing the spatial resolution from 0.25° to 0.1° to increase the local relevance of the precipitation estimates.

3. The inclusion of ocean areas, to enable oceanic studies and avoid missing data in coastal areas.

4. The addition of precipitation data from the NCEP-CFSR reanalysis, mainly to improve the performance in cold regions.

5. The addition of precipitation estimates derived from GridSat thermal infrared imagery for the pre-TRMM era to supplement the reanalysis and gauge data.

6. The addition of 0.1° daily interpolated gauge data to replace the coarse 0.5° CPC Unified and GPCC datasets.

7. The use of a daily gauge correction scheme that accounts for differences in gauge reporting times, to minimize timing mismatches when merging the daily gauge estimates with the satellite and reanalysis data.

8. Extension of the data record to 2016.

Version 1.2 (November 28, 2016)

Despite the many changes in version 1.2, the terrestrial precipitation estimates have not changed considerably since the previous version. The full list of changes is as follows:

1. MSWEP now also provides experimental precipitation estimates for ocean areas. When using MSWEP ocean data it should be kept in mind that: (i) the weights used for the temporal dynamics are almost entirely based on land stations which are not necessarily representative of ocean areas; (ii) the gauge-based data sources (CPC Unified and GPCC) are unavailable over ocean areas; and (iii) the estimates have not been validated (this is work in progress).

   For determining the long-term mean over ocean areas we could not use CHPclim as it only covers land areas. The long-term mean over ocean areas was therefore derived by weighting the long-term means of CMORPH, TMPA 3B42RT, GSMaP-MVK, ERA-Interim, and JRA-55. The weights for CMORPH, TMPA 3B42RT, and GSMaP-MVK were set to 1 for latitudes $< 25°$ and to 0 for latitudes $> 35°$. The weights decrease linearly from 1 at 25° to 0 at 35°. The weights for ERA-Interim and JRA-55 were set to 1. In the future, we intend to refine the weight estimates over ocean areas to obtain more reliable long-term means.

2. The record has been extended from 2014 to 2015.

3. ERA-Interim data were mistakenly offset by +3 hours in previous versions.

4. The threshold temperature for the inclusion of satellite data has been increased to 5°C for all time scales, to minimize the probability of incorporating potentially erroneous satellite data.

5. Satellite data prior to the year 2000 have been excluded. Among the satellite sources, only CMORPH provides data prior to 2000. However, the data were in lesser agreement with the gauge and reanalysis estimates and have therefore been excluded.

6. For generating the weight maps used for determining the temporal dynamics, the GHCN-D and GSOD station data are now normalized prior to the computation of grid-cell average time series.

7. The weight maps have been produced at 0.25° rather than 0.5°.

8. For each grid cell, rather than normalizing the satellite data, we rescaled the satellite data to match the reanalysis data for the period of overlap, to ensure retainment of the long-term trends.

Version 1.1 (August 2, 2016)

No changes to the actual data, the only changes are in the netCDF formatting. First, we changed the order of the variables from "lon, time, lat" to "time, lat, lon", which should solve some of the problems people have had with reading the data. Second, we corrected the time variable for the daily data, which was mistakenly offset by 1 day.

Version 1.0 (May 30, 2016)

Initial release corresponding exactly to the description in Beck et al. (2017).

6 Acknowledgements

By using MSWEP in any publication you agree to cite Beck et al. (2017). The dataset is being developed by Hylke Beck (Princeton University, Princeton, USA) in collaboration with Ming Pan, Eric Wood (Princeton University, Princeton, USA), Albert van Dijk (ANU, Canberra, Australia), Ad de Roo (JRC, Ispra, Italy), Vincenzo Levizzani (CNR-ISAC, Bologna, Italy), Jaap Schellekens (Deltares, Delft, The Netherlands), Diego Miralles (VU University Amsterdam, The Netherlands), and Brecht Martens (Ghent University, Ghent, Belgium). We gratefully acknowledge the precipitation dataset developers for producing and making available their datasets. The work was supported through IPA support for Hylke Beck from the U.S. Army Corps of Engineers' International Center for Integrated Water Resources Management (ICIWaRM), under the auspices of UNESCO, to further develop a Latin America and Caribbean Drought Monitor.

References

Akinremi, O. O., S. M. McGinn, and H. W. Cutforth (1999). Precipitation trends on the Canadian prairies. *Journal of Climate 12*(10), 2996–3003.

Beck, H. E., A. I. J. M. van Dijk, V. Levizzani, J. Schellekens, D. G. Miralles, B. Martens, and A. de Roo (2017). MSWEP: 3-hourly 0.25° global gridded precipitation (1979–2015) by merging gauge, satellite, and reanalysis data. *Hydrology and Earth System Sciences 21*(1), 589–615.

Beck, H. E., N. Vergopolan, M. Pan, V. Levizzani, A. I. J. M. van Dijk, G. P. Weedon, L. Brocca, F. Pappenberger, G. J. Huffman, and E. F. Wood (2017). Global-scale evaluation of 22 precipitation datasets using gauge observations and hydrological modeling. *Hydrology and Earth System Sciences Discussions*, 1–23.

Chen, M., W. Shi, P. Xie, V. B. S. Silva, V. E. Kousky, R. W. Higgins, and J. E. Janowiak (2008). Assessing objective techniques for gauge-based analyses of global daily precipitation. *Journal of Geophysical Research 113*, D04110.

Dee, D. P., S. M. Uppala, A. J. Simmons, P. Berrisford, P. Poli, S. Kobayashi, U. Andrae, M. A. Balmaseda, G. Balsamo, P. Bauer, P. Bechtold, A. C. M. Beljaars, L. van de Berg, J. Bidlot, N. Bormann, C. Delsol, R. Dragani, M. Fuentes, A. J. Geer, L. Haimberger, S. B. Healy, H. Hersbach, E. V. Hólm, L. Isaksen, P. Kallberg, M. Köhler, M. Matricardi, A. P. McNally, B. M. Monge-Sanz, J.-J. Morcrette, B.-K. Park, C. Peubey, P. de Rosnay, C. Tavolato, J.-N. Thépaut, and F. Vitart (2011). The ERA-Interim reanalysis: configuration and performance of the data assimilation system. *Quarterly Journal of the Royal Meteorological Society Part A 137*(656), 553–597.

Dirks, K. N., J. E. Hay, C. D. Stow, and D. Harris (1998). High-resolution studies of rainfall on Norfolk Island: Part II: Interpolation of rainfall data. *Journal of Hydrology 208*(3–4), 187–193.

Driouech, F., M. Déqué, and A. Mokssit (2009). Numerical simulation of the probability distribution function of precipitation over Morocco. *Climate Dynamics 32*(7), 1055–1063.

Fick, S. E. and R. J. Hijmans (2017). WorldClim 2: new 1-km spatial resolution climate surfaces for global land areas. *International Journal of Climatology in press*.

Funk, C., A. Verdin, J. Michaelsen, P. Peterson, D. Pedreros, and G. Husak (2015). A global satellite assisted precipitation climatology. *Earth System Science Data 7*, 275–287.

Garcia, M., C. D. Peters-Lidard, and D. C. Goodrich (2008). Spatial interpolation of precipitation in a dense gauge network for monsoon storm events in the southwestern United States. *Water Resources Research 44*, W05S13.

Goodison, B. E., P. Y. T. Louie, and D. Yang (1998). WMO solid precipitation intercomparison. Technical Report WMO/TD-872, World Meteorological Organization, Geneva.

Haylock, M. R., N. Hofstra, A. M. G. Klein Tank, E. J. Klok, P. Jones, and M. New (2008). A European daily high-resolution gridded data set of surface temperature and precipitation for 1950–2006. *Journal of Geophysical Research: Atmospheres 113*(D20).

Herold, N., L. V. Alexander, M. G. Donat, S. Contractor, and A. Becker (2016). How much does it rain over land? *Geophysical Research Letters 43*(1), 341–348.

Huffman, G. J., D. T. Bolvin, E. J. Nelkin, D. B. Wolff, R. F. Adler, G. Gu, Y. Hong, K. P. Bowman, and E. F. Stocker (2007). The TRMM Multisatellite Precipitation Analysis (TMPA): quasi-global, multiyear, combined-sensor precipitation estimates at fine scales. *Journal of Hydrometeorology 8*(1), 38–55.

Joyce, R. J., J. E. Janowiak, P. A. Arkin, and P. Xi (2004). CMORPH: A method that produces global precipitation estimates from passive microwave and infrared data at high spatial and temporal resolution. *Journal of Hydrometeorology 5*(3), 487–503.

Kang, S. and J.-B. Ahn (2015). Global energy and water balances in the latest reanalyses. *Asia-Pacific Journal of Atmospheric Sciences 51*(4), 293–302.

Knapp, K. R., S. Ansari, C. L. Bain, M. A. Bourassa, M. J. Dickinson, C. Funk, C. N. Helms, C. C. Hennon, C. D. Holmes, G. J. Huffman, J. P. Kossin, H.-T. Lee, A. Loew, and G. Magnusdottir (2011). Globally gridded satellite observations for climate studies. *Bulletin of the American Meteorological Society 92*(7), 893–907.

Kobayashi, S., Y. Ota, Y. Harada, A. Ebita, M. Moriya, H. Onoda, K. Onogi, H. Kamahori, C. Kobayashi, H. Endo, K. Miyaoka, , and K. Takahashi (2015). The JRA-55 reanalysis: General specifications and basic characteristics. *Journal of the Meteorological Society of Japan. Ser. I 93*, 5–48.

Lopez, P. (2007). Cloud and precipitation parameterizations in modeling and variational data assimilation: a review. *Journal of the Atmospheric Sciences 64*(11), 3766–3784.

Menne, M. J., I. Durre, R. S. Vose, B. E. Gleason, and T. G. Houston (2012). An overview of the Global Historical Climatology Network-Daily database. *Journal of Atmospheric and Oceanic Technology 29*(7), 897–910.

Nair, A. S. and J. Indu (2017). Performance assessment of Multi-Source Weighted-Ensemble Precipitation (MSWEP) product over India. *Climate 5*(1).

Schneider, U., A. Becker, P. Finger, A. Meyer-Christoffer, M. Ziese, and B. Rudolf (2014). GPCC's new land surface precipitation climatology based on quality-controlled in situ data and its role in quantifying the global water cycle. *Theoretical and Applied Climatology 115*(1), 15–40.

Schneider, U., P. Finger, A. Meyer-Christoffer, E. Rustemeier, M. Ziese, and A. Becker (2017). Evaluating the hydrological cycle over land using the newly-corrected precipitation climatology from the Global Precipitation Climatology Centre (GPCC). *Atmosphere 8*(3).

Sevruk, B., M. Ondrás, and B. Chvíla (2009). The WMO precipitation measurement intercomparisons. *Atmospheric Research 92*(3), 376–380.

Shepard, D. (1968). A two-dimensional interpolation function for irregularly-spaced data. In *ACM '68 Proceedings of the 1968 23rd ACM National Conference*, pp. 517–524.

Skok, G., N. Žagar, L. Honzak, R. Žabkar, J. Rakovec, and A. Ceglar (2015). Precipitation intercomparison of a set of satellite- and raingauge-derived datasets, ERA Interim reanalysis, and a single WRF regional climate simulation over Europe and the North Atlantic. *Theoretical and Applied Climatology 123*(1), 217–232.

Stephens, G. L., T. L'Ecuyer, R. Forbes, A. Gettelmen, J.-C. Golaz, A. Bodas-Salcedo, K. Suzuki, P. Gabriel, and J. Haynes (2010). Dreary state of precipitation in global models. *Journal of Geophysical Research: Atmospheres 115*(D24).

Sun, Y., S. Solomon, A. Dai, and R. W. Portmann (2006). How often does it rain? *Journal of Climate 19*(6), 916–934.

Trenberth, K. E., J. T. Fasullo, and J. Mackaro (2011). Atmospheric moisture transports from ocean to land and global energy flows in reanalyses. *Journal of Climate 24*(18), 4907–4924.

Trenberth, K. E. and Y. Zhang (in press). How often does it really rain? *Bulletin of the American Meteorological Society*.

Ushio, T., T. Kubota, S. Shige, K. Okamoto, K. Aonashi, T. Inoue, N. Takahashi, T. Iguchi, M. Kachi, R. Oki, T. Morimoto, and Z. Kawasaki (2009). A Kalman filter approach to the Global Satellite Mapping of Precipitation (GSMaP) from combined passive microwave and infrared radiometric data. *Journal of the Meteorological Society of Japan 87A*(II), 137–151.

Vila, D. A., L. G. G. de Goncalves, D. L. Toll, and J. R. Rozante (2009). Statistical evaluation of combined daily gauge observations and rainfall satellite estimates over continental South America. *Journal of Hydrometeorology 10*(2), 533–543.

Viney, N. R. and B. C. Bates (2004). It never rains on Sunday: the prevalence and implications of untagged multi-day rainfall accumulations in the Australian high quality data set. *International Journal of Climatology 24*(9), 1171–1192.

Weedon, G. P., G. Balsamo, N. Bellouin, S. Gomes, M. J. Best, and P. Viterbo (2014). The WFDEI meteorological forcing data set: WATCH Forcing Data methodology applied to ERA-Interim reanalysis data. *Water Resources Research 50*(9), 7505–7514.

Weedon, G. P., S. Gomes, P. Viterbo, W. J. Shuttleworth, E. Blyth, H. Österle, J. C. Adam, N. Bellouin, O. Boucher, and M. Best (2011). Creation of the WATCH forcing data and its use to assess global and regional reference crop evaporation over land during the twentieth century. *Journal of Hydrometeorology 12*(5), 823–848.

Xavier, A. C., C. W. King, and B. R. Scanlon (2016). Daily gridded meteorological variables in Brazil (1980–2013). *International Journal of Climatology 36*(6), 2644–2659.

Xie, P., M. Chen, S. Yang, A. Yatagai, T. Hayasaka, Y. Fukushima, and C. Liu (2007). A gauge-based analysis of daily precipitation over East Asia. *Journal of Hydrometeorology 8*(3), 607–626.

Xie, P., R. Joyce, S. Wu, S.-H. Yoo, Y. Yarosh, F. Sun, and R. Lin (2017). Reprocessed, bias-corrected CMORPH global high-resolution precipitation estimates from 1998. *Journal of Hydrometeorology in press*.

Zhang, L., W. R. Dawes, and G. R. Walker (2001). Response of mean annual evapotranspiration to vegetation changes at catchment scale. *Water Resources Research 37*(3), 701–708.

Zhang, W., M. Brandt, F. Guichard, Q. Tian, and R. Fensholt (2017). Using long-term daily satellite based rainfall data (1983–2015) to analyze spatio-temporal changes in the Sahelian rainfall regime. *Journal of Hydrology in press*.

Zolina, O., A. Kapala, C. Simmer, and S. K. Gulev (2004). Analysis of extreme precipitation over Europe from different reanalyses: a comparative assessment. *Global and Planetary Change 44*(1–4), 129–161.